ISSN 1392–1320 MATERIALS SCIENCE (MEDŽIAGOTYRA). Vol. 29, No. 1. 2023

The Investigation of Vortex Motion in the YBCO Devices Manufactured Utilizing a Gaussian-shaped Optical Spot from a Continuous-wave Laser

Artūras JUKNA

Photovoltaic Technologies Laboratory, Vilnius Gediminas Technical University (VILNIUS TECH), Sauletekio av. 3, Vilnius LT-10257, Lithuania

crossref http://dx.doi.org/10.5755/j02.ms.31099

Received 08 April 2022; accepted 03 May 2022

The current report focuses on the analysis of the investigation results of the Abrikosov vortex motion in the $YBa_2Cu_3O_{7-\delta}$ (YBCO) device, which is a *c*-axis textured $0.3 \times 50 \times 100$ μm^3 (thickness × width × length) stripe of YBCO superconductor deposited on a $LaAlO_3$ substrate. A laser beam focused in a Gaussian-shape optical spot of 5 μm in diameter modifies the stripe, initiating the oxygen out-diffusion and its uneven distribution in illuminated areas and in this way causing the appearance of a higher level of deoxygenation in the spot center and a lower level at its edges (slopes of weak superconductivity region). At temperatures below the temperature of the superconducting transition T_c, the current-self-produced magnetic field penetrates the optically modified area of the stripe in a form of Abrikosov magnetic vortices, and due to the current-self-produced Lorentz force, the vortices move toward their annihilation line resulting in energy dissipation. The vortices pinned on the slopes experience strong pinning and exert a magnetic drag force on moving vortices, which is confirmed by the stepped current-voltage dependences of the YBCO devices measured at temperatures $0.933 \cdot T_c \le T \le 0.958 \cdot T_c$. Our results demonstrate the advantages of partially deoxygenated YBCO material for the development of superconducting electronic devices with electronic properties controlled by the motion of Abrikosov vortices at temperatures below T_c of the superconductor.

Keywords: YBCO superconductor, partially deoxygenated cuprate, current-voltage characteristic, vortex motion.

1. INTRODUCTION

The temperature of the superconducting transition T_c [1], the critical current I_c [2], both critical magnetic fields [3, 4], and the resistivity *versus* temperature dependence [5] alter due to the variation in the oxygen concentration and oxygen ordering in the Cu-O basal planes of the crystalline structure of the $YBa_2Cu_3O_{7-\delta}$ (YBCO) superconductor. The residual oxygen content also predetermines the concentration of free carriers in CuO_2 planes [6] and is responsible for a structural transition from orthorhombic (at $\delta \sim 0$) to the tetragonal (at $\delta > 0.6$) phase at which the YBCO becomes an insulator [7]. When $0 < \delta < 0.6$, the interpretation of electrical and structural properties becomes complicated and somewhat ambiguous.

The type II superconductor at temperatures $T < T_c$ first obtains a mixed state (the state where the superconducting and non-superconducting (*i.e.* normal) phases co-exist in equilibrium) due to penetration of the magnetic field in the form of Abrikosov vortices [8, 9]. The magnetic vortices/antivortices nucleate at opposite edges of the superconducting film and, under the Lorentz force, move in a direction perpendicular to the direction of the bias current toward the center of the superconducting sample and annihilate there. At temperatures $T < T_c$, the first magnetic flux penetrates the YBCO superconductor through places of the weakest superconductivity, *i.e.* through the superconductor characterized by the lowest oxygen concentration that causes the lowest T_c and I_c of the material. The flux velocity depends on temperature and bias conditions as well as the F_L/F_p ratio. Here, F_L is the current self-produced Lorentz force, and F_p represents the pinning force produced by oxygen vacancies [10], defects in the bulk of the superconductor [11], or by the crystalline lattice mismatch between a superconducting film and its substrate [12]. Since the F_p strength depends on the origin of the pinning centers and predetermines the critical current of the superconductor, the control of pinning in YBCO is a crucial challenge in the search for new applications of thin films, as well as bulk superconductors in high-power electric, optoelectronic, [13] and magnetic devices [14].

The dissipation originated from the motion of Abrikosov magnetic vortices, leading to undesirable heating phenomena, especially in high-power applications [15]. In films wider than the effective penetration of the magnetic field [16], the Abrikosov vortices/antivortices nucleate at random places at the edge of the film and, under Lorentz force, wander between the strongest pining centers [17]. Due to the dissipation of the electric field power, the current-voltage (*I-V*) characteristic of a superconductor in the mixed state becomes nonlinear. When the current self-produced magnetic field and/or the external magnetic field exceed the second critical magnetic field of a superconductor [3], the *I-V* characteristic becomes linear because the material becomes normal (i.e. non-superconducting).

The present work reports on the results of the investigation of vortex motion in YBCO devices manufactured utilizing a green light beam from a continuous-wave laser. The testing devices are

* Corresponding author. Tel.: +370-5-2512462.
E-mail address: *arturas.jukna@vilniustech.lt* (A. Jukna)

$0.3 \times 50 \times 100$ μm^3 (thickness × width × length) stripes (*i.e.* much wider than the magnetic field penetration length into the YBCO superconductor [18]) provided with an artificially manufactured weak-superconductivity region in a form of a 5 μm wide and 50 μm long line of partially deoxygenated ($\delta \sim 0.2$) YBCO material. Due to the lower oxygen concentration, nonhomogeneous oxygen distribution, and diffusion in and out of the optically modified area, the weak superconductivity region under bias current significantly alters the electric properties of YBCO devices that express themselves as irregular, stepped, and wavered nonlinear *I-V* characteristics at temperatures $T < T_c$. Here, T_c is the critical temperature of the superconductor untreated by the laser.

2. DEVICE TECHNOLOGY

0.3 μm thick, epitaxial *c*-axis textured YBCO film was grown by a metalorganic chemical vapor deposition (MOCVD) technique [19] on optically transparent to green light and size of 10×10 mm^2 $LaAlO_3$ crystalline substrates. The films exhibited $T_c = 91.4$ K, the zero-resistivity temperature $T_{c0} = 91$ K, and the critical current density $J_c \sim 1.5$ MA/cm^2 at 78 K, estimated from the *I-V* dependences, which have been measured using the technique for the generation and measurement of repetitive current pulses of 10 ns duration [13].

Weak superconductivity regions were manufactured using a continuous wave Ar-ion laser light ($\lambda = 532$ nm) focused down to a spot size diameter of ~ 5 μm onto the YBCO surface, scanned at a speed of 50 μm/s utilizing a computer-controlled XY translation stage with a sample holder and a sample fixed on it. Manufacturing was processed in a dry nitrogen gas atmosphere by exposing the YBCO device to laser light with an output power of 0.4 W. The size of an optical spot on the surface of the YBCO film was measured directly using an optical microscope. At this optical power, the temperature of the illuminated areas increased to ~ 770 K; thus, this optical power of the laser activates the partial outflow of oxygen in the illuminated area, but does not destroy macroscopic superconductivity [20]. The geometry of each device on a $LaAlO_3$ substrate was processed at a laser power of 2.5 W and a beam translation speed of 5 μm/s. In this regime, the temperature of the illuminated areas increased above ~ 907 K [21], leading to a much more intensive oxygen out-diffusion, to $\delta > 0.6$, and to the orthorhombic-tetragonal structural transition in the YBCO material.

The schematic of the set of six 50×100 μm^2 YBCO superconducting devices is shown in Fig. 1. Four out of six devices were provided with a weak superconductivity region size of 5 μm in width and 50 μm in length, which was created by a laser beam. The remaining two devices were not treated by laser and did not contain an artificially oxygen-depleted region. Their characteristics were used as reference data to interpret the characteristics of the YBCO devices with a weak superconductivity region.

The residual oxygen content and the oxygen distribution profile in the artificial region of weak superconductivity of the YBCO devices were investigated at room temperature using a scanning electron microscope and an X-ray energy dispersive system measuring the chemical composition.

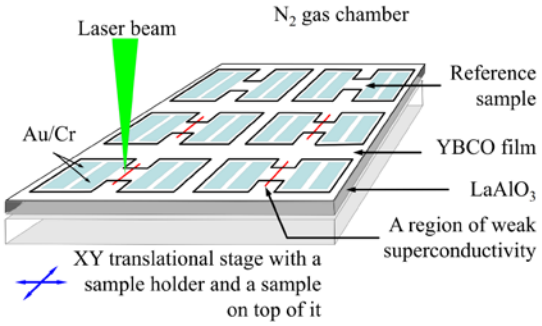

Fig. 1. The schematic of the set of six 50×100 μm^2 $YBa_2Cu_3O_{7-\delta}$ (YBCO) superconducting devices manufactured in the film on the size of 10×10 mm^2 $LaAlO_3$ substrates. Four out of six devices contain a 5 μm wide and 50 μm long artificially manufactured region of weak superconductivity with $\delta \sim 2$. The remaining two devices, which were not treated with laser, were left blank and used for reference purposes. Each device is provided with two large contact pads and contacts made of Au/Cr layers. The black lines represent the outer contours of the YBCO devices

The level of residual oxygen content was also indirectly estimated from the results of electric transport measurements of the YBCO devices, using a 4-probe technique at temperatures 80 K ≤ *T* ≤ 300 K.

3. EXPERIMENTAL RESULTS AND DISCUSSION

The resistivity *versus* temperature dependence at bias current $I = 1$ μA of YBCO device with an optically produced 5 μm wide and 50 μm long region of weak superconductivity is shown by curve 1 in Fig. 2.

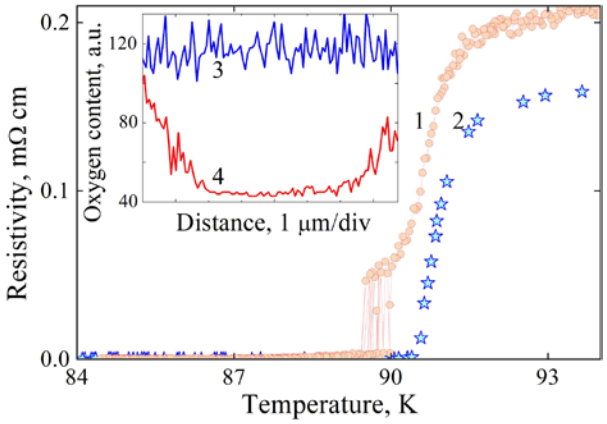

Fig. 2. Resistivity *versus* temperature dependence measured at bias current $I = 1$ μA for the YBCO device with a 5 μm wide and 50 μm long region of weak superconductivity (1) and without it (2). The inset represents the oxygen concentration (in arbitrary units) and oxygen distribution profile across the 5 μm wide weak superconductivity region, which was manufactured by the 0.4 W optical power from the green-light laser (4). Curve 3 represents the oxygen distribution profile on the reference device

Curve 2 (Fig. 2) represents the resistivity versus temperature dependence measured for the reference device.

At 1 μA bias current and zero external magnetic field, both devices exhibit the temperature of the superconducting transition T_c = 91.4 K since the superconducting transition taking place in the devices is related to the superconducting properties of the YBCO material not treated with laser.

The zero resistivity temperature T_{c0} of the optically modified device is much lower than T_c, indicating that the mixed state in the device is not stable and the level of dissipation of electric power depends on the electric properties of the oxygen-depleted region in the device. The transition from the mixed state to the superconducting state appears multiple times as a sharp drop of resistivity towards zero with a few repetitive recovering jumps to the value of ~ 0.05 mΩ·cm (Fig. 2).

The latter observation let us predict that the bias current self-produced magnetic field penetrates the type II superconductor in the region of weak superconductivity in the form of Abrikosov magnetic vortices/antivortices. Under the Lorentz force, the vortices and antivortices nucleate at the opposite edges of the stripe and move toward their annihilation line at its center, converting part of the electric energy into heat. Since magnetic vortices repel each other they should arrange themselves in a triangle magnetic lattice [22] with a lattice constant $a \sim \sqrt{\Phi_0/B}$. Here $\Phi_0 = 2.07 \times 10^{-15}$ Wb is the magnetic flux and B is the self-produced magnetic induction of the current. Magnetic induction penetrates the weak superconductivity region in the stripe with a number $n \sim B/\Phi_0$ of couples of Abrikosov vortices-antivortices. The density of magnetic vortices and their motion in the weak superconductivity region define the overall resistivity (Fig. 2) of the YBCO device.

The normal-state resistivity of our device with a partially deoxygenated region increased significantly compared to that of the reference device (Fig. 2). The $\delta \sim 0.2$ degrees of optically induced deoxygenation was estimated at room temperature using the scanning electron microscope, the X-ray energy dispersive system, and also using the room-temperature resistivity and the resistivity versus temperature dependences data for the normal-state YBCO films given, as discussed ref. [23, 24]. As it was predicted for the optical spot of Gaussian shape (inset of Fig. 2), the oxygen profile in the region of weak superconductivity is not uniform with the higher level of deoxygenation produced by optical power in the center of an optical spot and with a lower level of deoxygenation at the edges of the spot. This affects the formation of large slopes with a comparatively larger concentration of oxygen, resulting in the greater pinning force for magnetic flux penetrating them. On the slopes, the oxygen vacancies cannot compete with strong pinning centers (grain boundaries and screw dislocations), which are characteristic of the MOCVD-prepared YBCO films.

The easy vortex motion in the region of weak superconductivity is also evident in Fig. 3 a, showing the stepped *I-V* characteristics of a stripe with a weak superconductivity region. The stepped *I-V* characteristics were observed in a narrow range of temperatures ranging between 85.25 K ($0.933 \cdot T_c$) and 86.26 K ($0.944 \cdot T_c$) while the region of weak superconductivity stays in the mixed state. At temperature $T < 85.55$ K (curves 1 and 2 in Fig. 3) the steps in the *I-V* characteristics appear at $I < I_c$ of the superconducting device (a criterion for determining the I_c was used as an amplitude of the current resulting in the 10 μV voltage across the device).

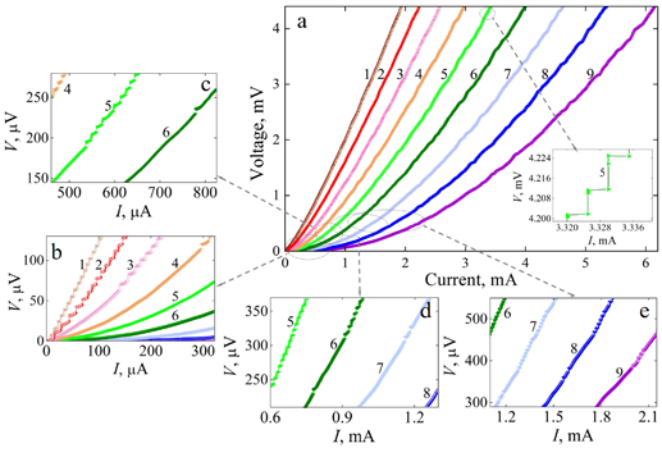

Fig. 3. a – current-voltage characteristics of a $0.3 \times 50 \times 100$ μm^3 YBCO stripe with an artificial region of weak superconductivity produced by a laser beam; b – e – curves 1 – 9 in extended scale showing the onset of the stepped *I-V* characteristic at different temperatures. All curves were obtained in the interval of temperatures $0.933 \le T/T_c \le 0.958$ with a temperature step of ~ 330 mK. The inset in the main figure represents a fragment of the *I-V* characteristic measured at T = 86.87 K = $0.950 \cdot T_c$ in the interval of current amplitudes 3.320 mA < I < 3.336 mA, near the limit of our measurement setup

With an increase in temperature, *i.e.* at $T > 85.55$ K (curves 3 – 9), the steps appear at current $I > I_c$.

Fig. 3 b presents the *I-V* characteristics at very low current biasing. We note that with decreasing temperature and increasing bias current, regularity in the step structure disappears (see curve 6 in Fig. 3 c – d and curves 7 – 9 in Fig. 3 d – e). Steps in the *I-V* characteristics appear when the $F_L \ge F_p$ for Abrikosov vortices in an artificially manufactured region of weak superconductivity in the YBCO stripe and give a clue that they correspond to different levels of energy dissipation in the device. The analysis of the results shown in Fig. 3 gives a clue that when vortices/antivortices are set to motion (when $F_L \ge F_p$), the level of energy dissipation increases (sudden increase in voltage in the *I-V* characteristic) and when vortices stop moving (when $F_L < F_p$), the level of energy dissipation decreases with a corresponding change in angle of the *I-V* characteristic.

In general, the pinning force, which is associated with various types of structural defects in the film, predetermines the character of the motion of Abrikosov magnetic vortices in superconductors. Extended growth defects, such as edge dislocations, twin planes, and grain boundaries, which depend mainly on the growth mode and stresses arising from the structural growth mismatch between the film and its substrate [19], behave as very efficient pinning centers. The dominant pinning centers in MOCVD films, used in the current experiment, are extended defects in the form of growth spirals with central screw dislocations [17, 25] and point defects such as oxygen vacancies in Cu-O_2 layers [26, 27]. Increasing the concentration of oxygen vacancies in the oxygen-deficient region of the stripe can affect the

suppression of superconducting parameters and the increase of a pinning for Abrikosov vortices. In the case of a *c*-axis-textured YBCO stripe containing a 5 μm wide oxygen depleted ($\delta \sim 0.2$) region being biased with a relatively strong current of several milliamps and locally heated by moving vortex bundles, oxygen diffusion along Cu-O chains (tracer diffusion) and oxygen diffusion from regions rich in oxygen to regions poor in oxygen (chemical diffusion) are very promising. This assumption is based on experimental results [28] showing that the oxygen activation energy along the grain boundaries in the YBCO film and the bulk of the material can be of the order of 0.21 – 0.37 eV and 0.45 eV – 0.86 eV [28], respectively, which are very close to current experimental conditions. The irregular steps observed in the *I-V* characteristics in the low bias current region (Fig. 3, curves 6 – 9) measured at low temperatures serve as an indicator of oxygen reordering in the Cu-O chains because of the electric field-assisted process of tracer diffusion of oxygen in the oxygen-depleted area. As shown in [6], tracer diffusion in oxygen-depleted YBCO can result in the formation of superconducting regions with a noticeably increased superconducting critical temperature T_c. This was explained by the formation of weak links in the oxygen-depleted area, resulting in granular superconductivity [6]. According to the above consideration, the electric field of current and the excess heat of moving vortices can make favorable conditions for oxygen reordering in the oxygen-depleted region of the YBCO strip causing a random elongation or shortening of Cu-O chains. Oxygen ordering in the Cu-O chains of the YBCO material can significantly contribute to the material's electric conductivity [29] and to the efficiency of the pinning for moving vortices [29, 30].

The resistivity of the YBCO stripe containing a weak superconductivity region is mainly predetermined by the level of energy dissipation due to vortex motion when this region is in the mixed state. The shape of nonlinear *I-V* dependences, measured at temperatures at which laser-untreated areas of the stripe are fully superconducting, varies with excess heating generated by moving vortices in the mixed state material. The shape of nonlinear *I-V* characteristics at large bias currents ($I > 0.5$ mA) becomes wavy (Fig. 3 a, c – e). The dynamic resistivity of the mixed state region in the YBCO strip changes in the range between ~ 55 μΩ·cm and ~ 70 μΩ·cm with a subsequent, quick recovery to the initial path. The wavy character of the *I-V* characteristics is attributable to variation in the concentration of moving vortex bundles, which generates different levels of energy dissipation in the mixed-state material in the YBCO stripes. The level of energy dissipation in mixed-state material depends on the ratio between the F_L and F_p amplitudes [23]. The F_L is almost linearly dependent on the bias current amplitude, but the F_p depends on many various factors related to the shape and homogeneity of the oxygen-depleted region, the escarpment of its slopes, and the dynamics of local temperature, which is, in its turn, related to the concentration and speed of moving vortices in this region. Energy dissipation can also be associated with chemical diffusion (diffusion due to oxygen gradients in the sample) and/or oxygen drift into the oxygen depleted region with $\delta \sim 0.2$ from the sample's fully-oxygenated regions ($\delta \sim 0$), as well as due to oxygen diffusion from the oxygen depleted region through grain boundaries [24] to laser untreated regions of the YBCO stripe. The oxygen tracer and chemical diffusion in and out of the oxygen-depleted region can sufficiently change the pining force for the moving vortices and, as a result, the total dissipation level in the YBCO stripe containing a narrow region of weak superconductivity.

4. CONCLUSIONS

Results of analysis of the stepped current-voltage characteristics observed in a range of temperatures $0.933 \le T/T_c \le 0.958$ of YBCO stripes with a region of weak superconductivity showed that the electric field of bias current together with a heat generated by the moving vortices might cause oxygen redistribution in the oxygen-depleted YBCO material. Oxygen redistribution via tracer diffusion (that is, spontaneous mixing of oxygen atoms in the Cu-O chains of the YBCO material) and chemical diffusion (due to oxygen concentration gradients) can contribute significantly to the electrical conductivity and the efficiency of the pinning force for moving vortices. Current results show that the motion of vortices is very sensitive to the temperature, bias current, and oxygen content of the YBCO superconducting film. A deeper understanding of the vortex motion mechanism in an oxygen-depleted ($\delta \sim 0.2$) region, which is manufactured using a beam from a continuous wave laser focused into a few micrometers wide optical spot of Gaussian shape, can open the way for new applications of YBCO superconducting films in superconducting electronic and optoelectronic devices for precise measurements of current, magnetic field, and/or temperature. Current results also show that, to use YBCO devices with a narrow region of weak superconductivity in high-power applications, the electric field of bias current and heat from moving vortices can initiate a chemical diffusion of oxygen from oxygen rich regions toward oxygen poor regions. Oxygen redistribution can significantly modify the oxygen distribution profile in the oxygen-depleted region, which is responsible for the electric properties of the YBCO device containing the oxygen-depleted region.

Acknowledgments

The author appreciates prof. R. Sobolewski (University of Rochester, USA) for useful discussions.

REFERENCES

1. **Cava, R.J., Batlogg, B., Chen, C.H., Rietman, E.A., Zahurak, S.M., Werder, D.** Single-Phase 60-K Bulk Superconductor in Annealed $Ba_2YCu_30_{7-\delta}$ ($0.3 < \delta < 0.4$) with Correlated Oxygen Vacancies in the Cu-O Chains *Physical Review B* 36 1987: pp. 5719 – 5722. https://link.aps.org/doi/10.1103/PhysRevB.36.5719
2. **Talantsev, E.F., Strickland, N.M., Wimbush, S.C., Storey, J.G., Tallon, J.L., Long, N.J.** Hole Doping Dependence of Critical Current Density in $YBa_2Cu_3O_{7-\delta}$ Conductors *Applied Physic Letters* 104 2014: pp. 242601 1 – 5. https://doi.org/10.1063/1.4883483

3. **Kokanović, I., Hills, D.J., Sutherland, M.L., Liang, R., Cooper, J.R.** Diamagnetism of $YBa_2Cu_3O_{6+x}$ Crystals Above T_c: Evidence for Gaussian Fluctuations *Physical Review B* 88 (6) 2013: pp. 060505(R) 1 – 6. https://doi.org/10.1103/PhysRevB.88.060505
4. **Grissonnanche, G., Cyr-Choinière, O., Laliberté, F., René de Cotret, S., Juneau-Fecteau, A., Dufour-Beauséjour, S., Delage, M.È., LeBoeuf, D., Chang, J., Ramshaw, B.J., Bonn, D.A., Hardy, W.N., Liang, R., Adachi, S., Hussey, N.E., Vignolle, B., Proust, C., Sutherland, M., Krämer, S., Park, J.H., Graf, D., Doiron-Leyraud, N., Taillefer, L.** Direct Measurement of the Upper Critical Field in Cuprate Superconductors *Nature Communications* 5 2014: pp 3280 1 – 8. https://doi.org/10.1038/ncomms4280
5. **Feenstra, R., Christen, D.K., Klabunde, C.E., Budai, J.D.** Role of Oxygen Vacancies in the Flux-Pinning Mechanism, and Hole-Doping Lattice Disorder in High-Current-Density $YBa_2Cu_3O_{7-x}$ Films *Physical Review B* 45 1992: pp. 7555(R) – 7558(R). https://link.aps.org/doi/10.1103/PhysRevB.45.7555
6. **Muroi, M., Street, R.** Charge Transfer, Phase Separation and Percolative Superconductivity in $YBa_2Cu_30_{6+y}$ *Physica C* 246 1995: pp. 357 – 374. https://doi.org/10.1016/0921-4534(95)00167-0
7. **Harabor, A., Rotaru, P., Harabor, N.A., Nozar, P., Rotaru, A.** Orthorhombic YBCO-123 Ceramic Oxide Superconductor: Structural, Resistive and Thermal Properties *Ceramics International* 45 2019: pp. 2899 – 2907. https://doi.org/10.1016/j.ceramint.2018.07.272
8. **D'Anna, G., Gammel, P.L., Safar, H., Alers, G.B., Bishop, D.J., Giapintzakis, J., Ginsberg, D.M.** Vortex-Motion-Induced Voltage Noise in $YBa_2Cu_3O_{7-\delta}$ Single Crystals *Physical Review Letters* 75 (19) 1995: pp. 3521 – 3524. https://link.aps.org/doi/10.1103/PhysRevLett.75.3521
9. **Henderson, W., Andrei, E.Y., Higgins, M.J., Bhattacharya, S.** Metastability and Glassy Behavior of a Driven Flux-Line Lattice *Physical Review Letters* 77 (10) 1996: pp. 2077 – 2080. https://link.aps.org/doi/10.1103/PhysRevLett.77.2077
10. **Atkinson, W.A.** $YBa_2Cu_3O_{7-\delta}$ Coated Conductor Cabling for Low AC-Loss and High-Field Magnet Applications* *Superconductor Science and Technology* 22 2 009: pp. 014005 1 – 5. https://doi.org/10.1088/0953-2048/22/6/065013
11. **Vodolazov, D.Yu., Ilin, K., Merker, M., Siegel, M.** Defect-Controlled Vortex Generation in Current-Carrying Narrow Superconducting Strips *Superconductor Science and Technology* 29 2016: pp. 025002 1 – 7. https://doi.org/10.1088/0953-2048/29/2/025002
12. **Deutscher, G.** Origin of Weak-Link Behavior of Grain Boundaries in Superconducting Cuprates and Pnictides *Applied Physics Letters* 96 (12) 2010: pp. 122502 1 – 3. https://doi.org/10.1063/1.3367723
13. **Jukna, A.** Superconducting Switch for High Power Pulse Antenna Excitation *Journal de Physique IV – Proceedings 11* 2001: pp. Pr11-151 – 155. https://doi.org/10.1051/jp4:20011124
14. **Wang, J., Wang, S.S., Zheng, J.** Recent Development of High Temperature Superconducting Maglev System in China *IEEE Transactions on Applied Superconductivity* 19 (3) 2009: pp. 2142 – 2147. https://ieeexplore.ieee.org/document/5166722
15. **White, J.S., Brown, S.P., Forgan, E.M., Laver, M., Bowell, C.J., Lycett, R.J., Charalambous, D., Hinkov, V., Erb, A., Kohlbrecher, J.** Observations of the Configuration of the High-Field Vortex Lattice in $YBa_2Cu_3O_7$: Dependence Upon Temperature and Angle of Applied Field *Physical Review B* 78 2008: pp. 174513 1 – 13. https://doi.org/10.1103/PhysRevB.78.174513
16. **Prozorov, R., Giannetta, R.W.** Magnetic Penetration Depth in Unconventional Superconductors *Superconductor Science and Technology* 19 2006: pp. R41 – R67. https://doi.org/10.1088/0953-2048/19/8/R01
17. **Wördenweber, R.** Mechanism of Vortex Motion in High-Temperature Superconductors *Reports on Progress in Physics* 62 1999: pp. 187 – 236. https://doi.org/10.1088/0034-4885/62/2/003
18. **El Hassan, A.A., Labrag, A., Taoufik, A., Bghour, M., El Ouaddi, H., Tirbiyine, A., Lmouden, B., Hafid, A., El Hamidi, H.** Magnetic Penetration Depth and Coherence Length in a Single-Crystal $YBa_2Cu_3O_{7-\delta}$ *Physica Status Solidi B* 258 2021: pp. 2100292 1 – 6. https://doi.org/10.1002/pssb.202100292
19. **Abrutis, A., Sénateur, J.P., Weiss, F., Kubilius, V., Bigelytė, V., Šaltytė, Z., Vengalis, B., Jukna, A.** Thin YBCO Films on $NdGaO_3$ (001) Substrates Grown by Injection MOCVD *Superconductor Science and Technology* 10 1997: pp. 959 – 965. https://doi.org/10.1088/0953-2048/10/12/021
20. **Jukna, A., Barboy, I., Jung, G., Abrutis, A., Li, X., Wang, D., Sobolewski, R.** Electric Transport Properties of $YBa_2Cu_3O_{7-\delta}$ Thin-Film Bridges with Laser-Written Channels of Easy Vortex Motion *Journal of Applied Physics* 99 2006: pp. 113902 1 – 5. https://doi.org/10.1063/1.2200595
21. **Xie, X.M., Chen, T.G., Wu, Z.L.** Oxygen Diffusion in the Superconducting Oxide $YBa_2Cu_3O_{7-x}$ *Physical Review B* 40 1989: pp. 4549 – 4556. https://link.aps.org/doi/10.1103/PhysRevB.40.4549
22. **Bishop, J.D., Gammel, P.L., Huse, D.A., Murray, C.A.** Magnetic Flux-Line Lattices and Vortices in the Copper Oxide Superconductors *Science* 255 1992: pp. 165 – 172. https://doi.org/10.1088/0034-4885/62/2/003
23. **Shams, G.A., Cochrane, J.W., Russell, G.J.** Thermal Transport in Polycrystalline $YBa_2Cu_3O_{7-\delta}$, Y_2BaCuO_5 and Melt-Processed $YBa_2Cu_3O_{7-\delta}$ Materials *Physica C: Superconductivity and its Applications* 351 (4) 2001: pp. 449 – 465. https://doi.org/10.1016/S0921-4534(00)01644-0
24. **Cava, R.J., Hewat, A.W., Hewat, E.A., Batlogg, B., Marezio, M., Rabe, K.M., Krajewski, J.J., Peck, Jr,W.F., Rupp, Jr,L.W.** Structural Anomalies, Oxygen Ordering and Superconductivity in Oxygen Deficient $Ba_2YCu_3O_x$ *Physica C: Superconductivity* 165 (5 – 6) 1990: pp. 419 – 433. https://doi.org/10.1016/0921-4534(90)90376-P
25. **Zhao, P., Ito, A., Kato, T., Yokoe, D., Hirayama, T., Goto, T.** High-J_c $YBa_2Cu_3O_{7-\delta}$ Superconducting Film Grown by Laser-Assisted Chemical Vapor Deposition Using a Single Liquid Source and its Microstructure *Superconductor Science and Technology* 26 2013: pp. 095016 1 – 5. https://doi.org/10.1088/0953-2048/26/9/095016
26. **Sun, H.B., Russel, G.J., Taylor, K.N.R.** Systematic Study of Pinning Energy for Oxygen-Deficient YBCO *Physica C: Superconductivity* 241 (3 – 4) 1995: pp. 219 – 22. https://doi.org/10.1016/0921-4534(94)02376-X

27. **Deutscher, G.** The Role of the Short Coherence Length in Unconventional Superconductors *Condensed Matter* 5 2020 pp. 77 1 – 4. https://doi.org/10.3390/condmat5040077

28. **Wang, T.G., Cao, J.J., Gou, X.F.** Activation Energy of Oxygen Diffusion: A Possible Indicator of Supercurrents Through $YBa_2Cu_3O_7$ Grain Boundaries *Applied Surface Science* 480 2019: pp. 765 – 769. https://doi.org/10.1016/j.apsusc.2019.02.208

29. **Osofsky, M.S., Cohn, J.L., Skelton, E.F., Miller, M.M., Soulen, Jr,R.J., Wolf, S.A., Vanderah, T.A.** Percolation Effects and Oxygen Inhomogeneities in $YBa_2Cu_3O_{7-\delta}$ Crystals *Physical Review B* 45 (9) 1992: pp. 4916 – 4929. https://link.aps.org/doi/10.1103/PhysRevB.45.4916

30. **Daeumling, M., Seuntjens, J., Larbalestier, D.** Oxygen-Defect Flux Pinning, Anomalous Magnetization and Intra-Grain Granularity in $YBa_2Cu_30_{7-\delta}$ *Nature* 346 1990: pp. 332 – 335. https://doi.org/10.1038/346332a0